

Lattice Boltzmann-Carleman quantum algorithm and circuit for fluid flows at moderate Reynolds number

Claudio Sanavio^{1, a)} and Sauro Succi¹

Fondazione Istituto Italiano di Tecnologia

Center for Life Nano-Neuroscience at la Sapienza

Viale Regina Elena 291, 00161 Roma, Italy

We present a quantum computing algorithm for fluid flows based on the Carleman-linearization of the Lattice Boltzmann (LB) method. First, we demonstrate the convergence of the classical Carleman procedure at moderate Reynolds numbers, namely for Kolmogorov-like flows. Then we proceed to formulate the corresponding quantum algorithm, including the quantum circuit layout and analyze its computational viability. We show that, at least for moderate Reynolds numbers between 10 and 100, the Carleman-LB procedure can be successfully truncated at second order, which is a very encouraging result. We also show that the quantum circuit implementing the single time-step collision operator has a fixed depth, regardless of the number of lattice sites. However, such depth is of the order of ten thousands quantum gates, meaning that quantum advantage over classical computing is not attainable today, but could be achieved in the near-mid term future. The same goal for the multi-step version remains however an open topic for future research.

^{a)}Electronic mail: claudio.sanavio@iit.it

I. INTRODUCTION

Quantum computing¹ holds promise to provide dramatic speed up to the solution of a number of major scientific problems, including advanced industrial and societal applications^{2–5}. The so-called quantum advantage stems from the deepest (and most counterintuitive) features of quantum mechanics, in particular, superposition and entanglement of quantum states which offer, at least in principle, the chance to exploit the full Hilbert space, scaling exponentially with the number of qubits, the smallest bit of quantum information. This feature provides a natural way out to the infamous "curse of dimensionality", plaguing the simulation of most quantum many-body problems, both classical and quantum^{6,7}.

Yet, realizing such a mind-boggling potential faces with a number of steep challenges, both conceptual and technological, primarily fast decoherence and, even more so, the quantum noise affecting the operation of real-life quantum computers. Understandably, quantum computing to date has been directed mostly to quantum physics problems, featuring a one to one mapping between the physical system to be simulated and the quantum hardware⁸. Yet, there is a mounting interest in learning whether the potential of quantum computing can be put at use also for solving the most compelling problems in classical physics, as typically described by strongly nonlinear partial differential equations^{9–13}. In this respect, fluid turbulence stands out as a prominent candidate, both in terms of fundamental physics and also in view of its pervasive applications in both natural and industrial phenomena.

This work inscribes precisely within the aforementioned scenario; we shall present a quantum algorithm, and the associated circuit, solving the basic (Navier-Stokes) equations which govern the physics of dissipative fluids. For reasons to be apparent in the sequel, our strategy is based on the Lattice Boltzmann formalism for fluid flows.

The paper is organized as follows. In Section II we introduce the classical equation of motions. In Section III we review the lattice Boltzmann method. In Section IV we focus on the Carleman linearization. We introduce two ways to deal with the infinite number of variables, and we show how to conveniently cut down the size of the system of equations. We then show in Section V an explicit analysis of the CL method and its performance on a classical computer. In Section VI we define the embedding of the Carleman variables into the space of qubits and we explicitly construct the quantum circuit. This consists of two separate steps, to be applied in series, the collision and the multi-streaming operator.

Finally, in Section VII we draw preliminary conclusions and draw a prospective outlook for future works in this area.

II. THE EQUATION OF MOTION OF CLASSICAL FLUIDS

The Navier-Stokes equations (NSE), read as follows:

$$\partial_t \rho + \partial_a (\rho u_a) = 0 \quad (1)$$

$$\partial_t (\rho u_a) + \partial_b (\rho u_a u_b) = -\partial_a p + \partial_b \sigma_{ab} + F_a \quad (2)$$

with u_a being the macroscopic velocity of the fluid, ρ the fluid density, F_a the external force, p the pressure of the fluid and σ_{ab} the dissipative tensor. The latin indices a, b run over the cartesian coordinates x, y and z . The first line (1) is the continuity equation, whereas the second line (2) is a vectorial representation of the evolution of the macroscopic velocities. We use here the Einstein convention, by which repeated indices are summed upon. Eqs. (2) are non-linear partial differential equations, and the strength of the non-linearity bears heavily on our ability to solve the NSE, either analytically, or even using the most advanced computational fluid dynamics (CFD) methods¹⁴.

The Reynolds number Re is a measure of the non-linearity of the system and it is defined as the ratio between the inertial and viscous forces, $Re = u \cdot \nabla u / \nu \nabla^2 u$, as given by the ratio:

$$Re = \frac{|u|L}{\nu}, \quad (3)$$

where $|u|$ is the magnitude of the macroscopic velocity and L is the global system size. To be noted that the Reynolds number takes on very large numbers also under very mundane conditions, an ordinary car moving at a standard speed already features $Re \sim 10^7$, ten millions. Given that the computational complexity of fluid turbulence scales like Re^3 , this means that 10^{21} active degrees of freedom need to be tracked in order to simulate the dynamics of a full car. With order thousands floating point operation per degree of freedom, this yields 10^{24} floating point operations, implying 10^6 CPU/GPU seconds, about two weeks, to complete the simulation on an ideal Exascale computer. So much for an ordinary car. Consider now the problem of numerical weather forecast, which implies Reynolds numbers easily in the order of 10^{10} , leading to an intractable problem for any foreseeable classical

computer. These simple figures speak clearly for the motivation to investigate the possibility of exploiting quantum computers for simulating classical turbulence¹⁵.

CFD is a traditional forefront of computational science, with a ceaseless quest for better and more efficient computational methods. In the last three decades, the Lattice Boltzmann method (LBM) , has gained a prominent role in the CFD arena¹⁶⁻²¹. In a nutshell, LBM is a stylized version of the Boltzmann equation which retains the essential physics of fluids within a very efficient computational kinetic-theory harness.

It consists of two basic processes: streaming, by which particles move freely from one lattice site to the next, and collisions, whereby particles exchange mass, momentum and energy, so as to sustain the collective dynamics telling fluids apart from a "wild bunch" of independent particles. The streaming is minimally non local, as it connects single-cell neighbors, but linear, in fact *exact*, as no information is lost in moving information from one lattice site to another. Conversely, collisions hold the (quadratic) nonlinearity of the physics of fluids, but in a local form, because, consistently with Boltzmann's kinetic theory, only particles in the same lattice site interact with each other. This clearcut separation between nonlinearity and nonlocality is possibly the most profound hallmark of the LBM, and the basic reason for its computational success especially on parallel computers. It is therefore reasonable to investigate whether the advantages of this clearcut separation carries on to the quantum computing scenario.

At a superficial glance, the prospects of using a quantum computer for CFD look promising. The number of qubits, q , required to store Re^3 dynamic degrees of freedom is simply given by:

$$q = 3\log_2 Re \sim 10\log_{10} Re \quad (4)$$

This shows that $q \sim 70$ qubits are in principle sufficient to quantum-simulate a car. And even numerical weather forecast, say $Re \sim 10^{10}$ could be quantum-simulated with about $q \sim 100$ qubits, well within the *nominal* capability of current quantum hardware²².

As mentioned above, many hurdles stand in the way of this blue-sky scenario. Leaving aside the notorious issues of quantum noise and decoherence, in the following we focus on two issues which are specific to classical fluids: nonlinearity and dissipation.

Indeed, the dynamics described by Eqs. (1),(2) is nonlinear and subject to dissipation, whereas quantum algorithms consist into the application of a sequence of unitary, hence conservative, operators. This fundamental difference represents a serious obstacle to the

formulation of a quantum algorithm capturing the NSE dynamics.

A possible solution is provided by Carleman Linearization (CL)^{23–25}. This is a general strategy to transform a non-linear equation into an infinite set of linear equations, promoting all the different monomials appearing in the nonlinear equation to independent variables. In order to numerically deal with the infinite newly-defined variables, a truncation is applied at a given problem-dependent level.

CL removes the first obstacle to the resolution of the NSE through quantum computers, non-linearity. Better said, it trades nonlinearity for extra-dimensions and nonlocality, as it will become apparent shortly. To deal with the non-conservative part, we can use an extended circuit, first proposed in²⁶, that makes use of an ancilla qubit to mimic the dissipative dynamics.

Various Carleman-based LBM schemes have been proposed in the recent literature^{13,27,28}, but, to the best of our knowledge, none of them provided an explicit description of the corresponding quantum circuit.

III. THE LATTICE BOLTZMANN METHOD

The LBM has been proved particularly efficient to simulate the NSE, both at low and high Reynolds number²⁹. LBM models the system in a d dimensional regular lattice and defines Q vectorial velocities c_i pointing toward the neighboring sites. The probability distribution functions $f_i(x, t)$, with $i = 0, \dots, Q - 1$ represent the probability of a representative fluid particle at lattice site x at time t of having velocity c_i . The vector notation is relaxed for simplicity.

The distribution functions are related to the macroscopic quantities fluid density ρ and fluid velocity u by the linear relations:

$$\rho(x, t) = \sum_{i=0}^{Q-1} f_i(x, t), \quad (5)$$

$$\rho(x, t)u(x, t) = \sum_{i=0}^{Q-1} c_i f_i(x, t), \quad (6)$$

where the discretized velocities c_i are vectors with components either $-1, 0$ or 1 , see Table I and Fig. 1 for an explicit example in $D = 2$ and $Q = 9$.

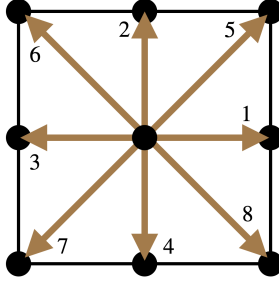


FIG. 1. The D2Q9 model. The model is defined on a two-dimensional square lattice, with the corresponding set of nine velocity vectors labeled by index, cf. Table I.

i	0	1	2	3	4	5	6	7	8
w_i	4/9	1/9	1/9	1/9	1/9	1/36	1/36	1/36	1/36
c_i	(0, 0)	(1, 0)	(0, 1)	(-1, 0)	(0, -1)	(1, 1)	(-1, 1)	(-1, -1)	(1, -1)

TABLE I. The weights and velocity set of the D2Q9 model.

The lattice Boltzmann equation (LBE) reads as follows^{30,31}:

$$f(x + c_i, t + 1) - f_i(x, t) = -\Omega_i \quad \text{for } i = 0, \dots, Q - 1. \quad (7)$$

where the left hand side is the free streaming along the i -th direction and the left hand side is the discrete-velocity collision operator. The time step has made unity for simplicity.

It proves expedient to use the Bhatnagar–Gross–Krook (BGK) relaxation expression of the collision term

$$\Omega_i = -\frac{1}{\tau}(f_i - f_i^{\text{eq}}) \quad (8)$$

where τ is the relaxation time-scale and the local equilibrium f_i^{eq} is defined through a Taylor expansion of the Boltzmann equilibrium distribution, as follows:

$$f_i^{\text{eq}}(x, t) = w_i \rho(x, t) \left(1 + \frac{u \cdot c_i}{c_s^2} + \frac{(u \cdot c_i)^2}{2c_s^4} - \frac{u \cdot u}{2c_s^2} \right), \quad (9)$$

where c_s is the lattice speed of sound, typically $1/\sqrt{3}$ for most lattices. The weights w_i can be obtained from the expansion of the equilibrium function (9) in terms of Hermite

polynomials and depend on the number of dimensions D and discrete velocities Q . They are reported in Table I for the D2Q9 model.

The dynamics ruled by Eq. (7) consists of two computational steps. First, the collision step is given by a local and non-linear operation that transforms the pre-collisional state $f_i(x, t)$ into the post-collisional one $f_i^*(x, t)$, as follows:

$$f_i^*(x, t) = (1 - \omega)f_i(x, t) + \omega f_i^{\text{eq}}, \quad (10)$$

where we have used the BGK form of the collision operator, and defined $\omega = \frac{\Delta t}{\tau}$, with Δt being the time step of the evolution. From Eq. (10) we see that if $\omega = 1$ the system collapses to the local equilibrium at each time step. In general, LBM allows values of $\omega < 2$ for matter of (linear) stability.

Second, the streaming step shifts the density functions to the nearest-neighbor site, as

$$f_i(x + c_i, t + \Delta t) = f_i^*(x, t). \quad (11)$$

The streaming process represents the free-motion of the fluid parcel across the lattice. Notice that the particles always land on a lattice site.

A. Weakly compressible limit

For weakly-compressible flows, the density can be taken as nearly constant, with a value $\rho \approx 1$. This allows to write $\frac{1}{\rho} \sim (2 - \rho)$, which permits to write the equilibrium function (9) as a cubic function of the density distributions, namely:

$$f_i^{\text{eq}} = L_{ij}f_j + Q_{ijk}f_jf_k + T_{ijkl}f_jf_kf_l, \quad (12)$$

with the linear, quadratic and cubic operators defined as

$$\begin{aligned} L_{ij} &= w_i \left(1 + \frac{c_i \cdot c_j}{c_s^2} \right), \\ Q_{ijk} &= \frac{w_i}{c_s^4} (c_i \cdot c_j c_i \cdot c_k - c_s^2 c_j \cdot c_k), \\ T_{ijkl} &= -\frac{1}{2} Q_{ijk}, \quad \forall l. \end{aligned} \quad (13)$$

The collision step can then be rewritten in mode-coupling form as follows:

$$f_i^* = A_{ij}f_j + B_{ijk}f_jf_k + C_{ijkl}f_jf_kf_l, \quad (14)$$

where the matrices A , B and C are obtained from the previous operators via the relations

$$\begin{aligned} A_{ij} &= (1 - \omega)\delta_{ij} + \omega L_{ij}, \\ B_{ijk} &= \omega Q_{ijk}, \\ C_{ijkl} &= -\frac{\omega}{2}Q_{ijk}, \quad \forall l. \end{aligned} \quad (15)$$

To be noted that the nonlinearity is formally carried out by the Mach number $\mathbf{Ma} = u/c_s$ which is $O(1)$, in stark contrast with the Reynolds number, easily in the multimillions for macroscopic objects, e.g. a standard automobile. This is a potentially major advantage over the continuum formulation of fluid dynamics.

IV. THE CARLEMAN LINEARIZATION

As noted earlier on, the Carleman linearization²³ transforms a finite-dimensional non-linear problem into an infinite set of linear equations. This technique makes the problem more suited to quantum computers, as the quantum mechanics of a closed system relies on linear algebra (leaving aside the measurement problem, of course). It consists of assigning the status of independent dynamic variable to any of the monomials in Eq. (14), thus defining the non-local variables $g_{ij}(x_1, x_2) \equiv f_i(x_1)f_j(x_2)$, $h_{ijk}(x_1, x_2, x_3) \equiv f_i(x_1)f_j(x_2)f_k(x_3)$, and so on for the higher degrees polynomials. We sketch an example of these functions in Figure 2.

We then define the Carleman vector $V = (f_0(x_1), \dots, g_{00}(x_1, x_1), \dots, h_{Q-1,Q-1,Q-1}(x_N, x_N, x_N), \dots)$ as the vector including all the possible products of functions f localized at each of the N lattice sites. The Carleman system is an infinite-dimensional set of linear equations, which can symbolically be written as:

$$V^* = \mathcal{C}V, \quad (16)$$

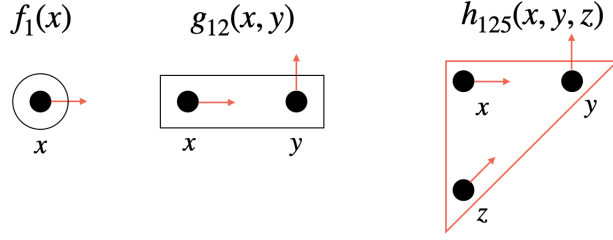


FIG. 2. An example of the Carleman variables of first, second and third order f , g and h respectively. In the above, $f_1(x)$ is the local variable in x with velocity c_1 , $g_{12}(x, y) = f_1(x)f_2(y)$ is the non-local variable of the second order with velocities c_1 at lattice site x and c_2 at lattice site y . Finally, $h_{125}(x, y, z) = f_1(x)f_2(y)f_5(z)$ is the three-point non-local variable obtained by multiplication of the three functions located in x, y and z with velocities c_1, c_2 and c_5 , respectively.

where V^* is the Carleman vector after collision, and \mathcal{C} is the Carleman matrix, whose components can be obtained by Eq. (14).

In the following, we consider two different procedures for dealing with the infinite number of Carleman variables, truncation and closure.

A. Carleman truncation

We ignore the higher degree terms by applying a truncation to the Carleman system, by simply neglecting the terms with degree above the order of the truncation.

1. Second order Carleman truncation

At 2nd order, all the terms with degree 3 or higher are set to zero, ($h = 0$). Thus, we write:

$$f_i^*(x_1) = A_{ij}f_j(x_1) + B_{ijk}g_{jk}(x_1, x_1), \quad (17)$$

$$g_{ij}^*(x_1, x_2) = A_{ik}A_{jl}g_{kl}(x_1, x_2).$$

Therefore, the Carleman system can be written in terms of the vector $V_{\text{tr}}^{(2)}$, which collects all the components of f and g at each lattice site, and the corresponding vector after collision

$V_{\text{tr}}^{(2)*}$. The linear relation between the two is given by the matrix $\mathcal{C}_{\text{tr}}^{(2)}$ that collects the elements from Eq. (17).

2. *Third order Carleman truncation*

With the truncation at 3rd order, the Carleman equations read as follows:

$$\begin{aligned} f_i^*(x_1) &= A_{ij}f_j(x_1) + B_{ijk}g_{jk}(x_1, x_1) + C_{ijkl}h_{jkl}(x_1, x_1, x_1), \\ g_{ij}^*(x_1, x_2) &= A_{ik}A_{jl}g_{kl}(x_1, x_2) + A_{ik}B_{jlm}h_{klm}(x_1, x_2, x_2) + B_{ikl}A_{jm}h_{klm}(x_1, x_1, x_2), \\ h_{ijk}^*(x_1, x_2, x_3) &= A_{il}A_{jm}A_{kn}h_{lmn}(x_1, x_2, x_3). \end{aligned} \quad (18)$$

B. Carleman closure

We propose an alternative and slightly more accurate method to cut down the number of Carleman variables. We approximate the product of d functions f to the product of $d-1$ functions multiplied by a constant. We choose this constant to be the LBM weight of the corresponding index that has been removed, thereby approximating the function with its steady equilibrium value.

1. *Second order Carleman closure*

We give here an explicit example of the closure procedure at second order approximating the following third order polynomial as

$$\begin{aligned} f_i(x_1)f_j(x_2)f_k(x_3) &= \frac{1}{3}[f_i(x_1)g_{jk}(x_2, x_3) + f_j(x_2)g_{ik}(x_1, x_3) + f_k(x_3)g_{ij}(x_1, x_2)] \\ &\approx \frac{1}{3}[w_i g_{jk}(x_2, x_3) + w_j g_{ik}(x_1, x_3) + w_k g_{ij}(x_1, x_2)]. \end{aligned} \quad (19)$$

At this order, the closure affects directly the definition of the equilibrium function, as the term $C_{ijkl}f_jf_kf_l$ changes and the closure leads to

$$\begin{aligned}
f_i^* &= A_{ij}f_j + B_{ijk}f_jf_k + C_{ijkl}f_jf_kf_l \\
&= A_{ij}f_j + B_{ijk}f_jf_k + \frac{1}{3}C_{ijkl}\left(w_jf_kf_l + w_kf_jf_l + w_lf_jf_k\right) \\
&= A_{ij}f_j + \frac{5}{6}B_{ijk}f_jf_k,
\end{aligned} \tag{20}$$

where the last line has been obtained via the relations

$$\begin{aligned}
C_{ijkl}w_j &= C_{ijkl}w_k = 0, \\
C_{ijkl}w_l &= -\frac{B_{ijk}}{2}.
\end{aligned} \tag{21}$$

The Carleman form of the LBE after closure at second order is given by:

$$f_i^*(x_1) = A_{ij}f_j(x_1) + \frac{5}{6}B_{ijk}g_{jk}(x_1, x_1) \tag{22}$$

$$g_{ij}^*(x_1, x_2) = A_{ik}A_{jl}g_{kl}(x_1, x_2) + \frac{5}{18}[w_iB_{jkl}g_{kl}(x_2, x_2) + w_jB_{ikl}g_{kl}(x_1, x_1)]. \tag{23}$$

We see that the closure makes the collision step *non-diagonal*, as it involves g functions located at different sites.

2. *Third order Carleman closure*

Closure at third or higher order does not change the equilibrium function. The combination of four distribution functions is approximated to

$$\begin{aligned}
f_i(x_1)f_j(x_2)f_k(x_3)f_l(x_4) &\approx \frac{1}{4}[w_ih_{jkl}(x_2, x_3, x_4) + w_jh_{ikl}(x_1, x_3, x_4) + w_kh_{ijl}(x_1, x_2, x_4) \\
&\quad + w_lh_{ijk}(x_1, x_2, x_3)].
\end{aligned} \tag{24}$$

The collision step becomes:

$$\begin{aligned}
f_i^*(x_1) &= A_{ij}f_j(x_1) + B_{ijk}g_{jk}(x_1, x_1) + C_{ijkl}h_{jkl}(x_1, x_1, x_1), \\
g_{ij}^*(x_1, x_2) &= A_{ik}A_{jl}g_{kl}(x_1, x_2) + A_{ik}B_{jlm}\left(\frac{7}{8}h_{klm}(x_1, x_2, x_2) + \frac{1}{4}w_i \sum_n h_{lmn}(x_2, x_2, x_2)\right) \\
&\quad + B_{ikl}A_{jm}\left(\frac{7}{8}h_{klm}(x_1, x_1, x_2) + \frac{1}{4}w_j \sum_n h_{lmn}(x_1, x_1, x_1)\right) \\
h_{ijk}^*(x_1, x_2, x_3) &= A_{il}A_{jm}A_{kn}h_{lmn}(x_1, x_2, x_3) + \\
&\quad \frac{1}{4}[w_iA_{jl}B_{kmn}h_{lmn}(x_2, x_3, x_3) + w_jA_{il}B_{kmn}h_{lmn}(x_1, x_3, x_3)] \\
&\quad + \frac{1}{4}[w_iB_{jlm}A_{kn}h_{lmn}(x_2, x_2, x_3) + w_kA_{il}B_{jmn}h_{lmn}(x_1, x_2, x_2)] \\
&\quad + \frac{1}{4}[w_jB_{ilm}A_{kn}h_{lmn}(x_1, x_1, x_3) + w_kB_{ilm}A_{jn}h_{lmn}(x_1, x_1, x_2)] \\
&\quad + \frac{1}{32} \sum_n \left(w_iw_jB_{klm}h_{lmn}(x_3, x_3, x_3) \right. \\
&\quad \left. + w_iw_kB_{jlm}h_{lmn}(x_2, x_2, x_2) + w_jw_kB_{ilm}h_{lmn}(x_1, x_1, x_1) \right).
\end{aligned}$$

V. COMPARISON BETWEEN THE EXACT LBM AND THE CARLEMAN LINEARIZED MODEL

In this section, we present the simulations of a two dimensional system with constant pressure and no external forces. We consider a Kolmogorov-like flow on a grid of $N = N_x N_y$ points. The distribution functions are initialized as follows:

$$f_i(x, y) = w_i \left[1 + A_x \cos \left(\frac{2\pi}{N_y} k_{xy} \right) c_i \cdot c_1 + A_y \cos \left(\frac{2\pi}{N_x} k_y x \right) c_i \cdot c_2 \right], \quad (25)$$

where the wave numbers $k_{x,y}$ are integers and $A_{x,y}$ is a positive amplitude between 0 and 1.

By setting $A_y = 0$, the velocity in the y direction is null, $u_y = 0$ and the dynamics is purely linear and dissipative, as the convective term vanishes, $u \cdot \nabla u = 0$. The dynamics is then ruled only by the linear term $\nu \nabla^2 u$. In this regime, the velocity u_x evolves following an exponential decaying function, with $u_x(t) = u_x(0) \exp\{-\nu k^2 t\}$, with the viscosity ν being a function of the LBM parameter ω ,

$$\nu = \frac{1}{6} \left(\frac{2}{\omega} - 1 \right), \quad (26)$$

in lattice units with $\Delta t = \Delta x = 1$. For this linear regime, we show in Fig. 3(a) the velocity at $t = 0$ for a grid with $N = 32 \times 32$, choosing $A_k = 0.3$ ($u_x = 0.1$) and $k_x = 1$. Simulations using the “exact” LBM recover the exponential decay, as shown in Fig. 3(b) for different values of ω .

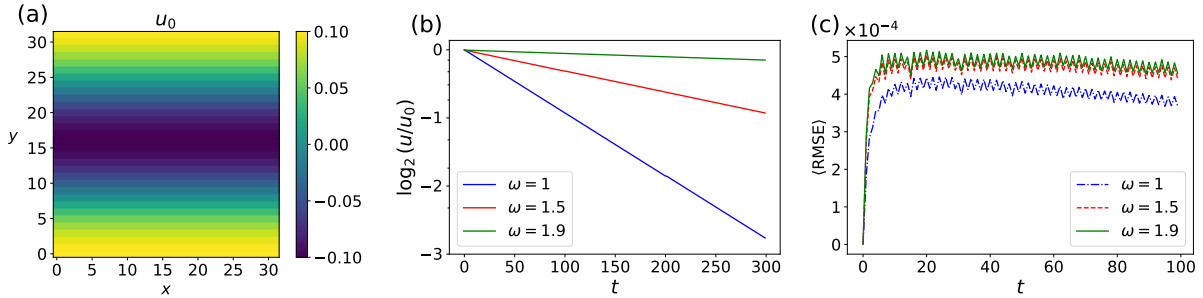


FIG. 3. In (a) the initial conditions of the Kolmogorov flow on a grid with 32×32 grid points, with $k_x = 1$, $A_x = 0.3$. In (b) The exponential decay of the macroscopic quantity u_x for different choices of ω , the exponent of the decay follows Eq. (26). In (c) the relative root mean squared error defined in Eq. eqrefeq:RRMSE between the results obtained by LBM and by Carleman linearization truncated at second order.

In order to compare the LBM with the CL approximation, we define the Root Mean Squared Error (RMSE) $\epsilon(a, b)$ between two distributions a and b as

$$\epsilon(a, b) = \sqrt{\sum_{i=1}^N \frac{1}{N} \left(\frac{a_i - b_i}{a_i} \right)^2}. \quad (27)$$

In the above, N is the number of grid points. Accordingly, we end up with one RMSE for each of the Q velocity directions of the LBM. In our analysis, we consider the mean value of the RMSE among the Q distributions, namely:

$$\langle \text{RMSE} \rangle = \sum_{q=0}^{Q-1} \frac{1}{Q} \epsilon(f_q^{\text{LBM}}, f_q^{\text{CL}}), \quad (28)$$

where $f_q^{\text{LBM}}, f_q^{\text{CL}}$ are the distribution functions calculated with the LBM and the CL respectively. The quantity $\langle \text{RMSE} \rangle$ accounts for the mean deviation of the CL with respect to the results obtained by the LBM. From Fig. 3(c), we see that this deviation is of the order of 10^{-4} . This is fully consistent with the weak compressibility error of the standard LBM.

Upon increasing the value of A_y , we start observing the effects of the non-linearity, as the convective terms raises in magnitude and the Reynolds number becomes larger. Thus, the temporal evolution of u_x and u_y deviates from the exponential decay, as it is shown in Figure 4(a), with parameters $A_x = 0.3$, $k_x = 1$, $A_y = 0.2$, $k_y = 4$. For low ω (high dissipation, low Reynolds) the curves rapidly go back to the original decaying dynamics, whereas for $\omega = 1.9$, the deviation is evident even after longer time periods. The oscillations of the curve are due to the presence of small vortices caused by the mildly turbulent dynamics.

In Fig. 4(b) we compare the $\langle \text{RMSE} \rangle$ between the truncation and the closure at second order. The Figure refers to $\omega = 1.5$, but similar deviations are obtained for different ω , as it is evident from Fig. 4(c). We see that the approximation brought by the closure leads to a lower $\langle \text{RMSE} \rangle$, thus mitigating the error. However, we notice that the order of magnitude between the two cut-off methods remains the same. The $\langle \text{RMSE} \rangle$ depends on the value of ω , as shown in Fig. 4(c), and therefore on the corresponding value of the Reynolds number Re . At low Reynolds the $\langle \text{RMSE} \rangle$ remains below 10^{-3} , which is a noteworthy result given the small number of grid-points employed in these simulations.

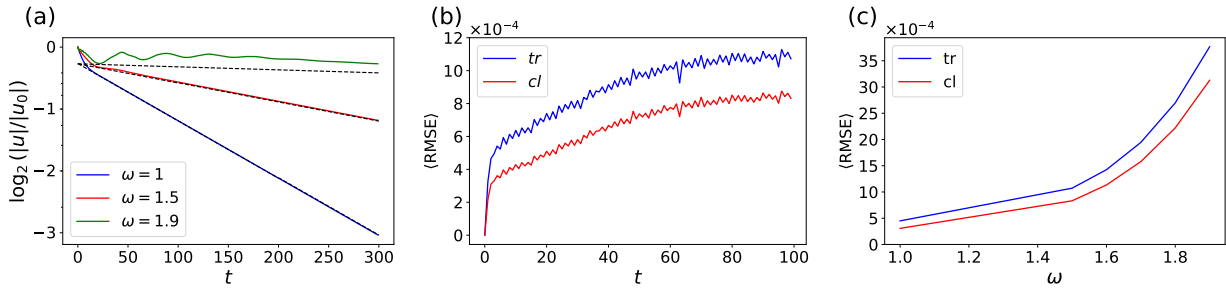


FIG. 4. (a) The temporal evolution of u_x for different values of ω with initial conditions $A_x = 0.3$, $A_y = 0.2$, $k_x = 1$, and $k_y = 4$, (b) the comparison between the $\langle \text{RMSE} \rangle$ of the truncation method (with label 'tr') and the $\langle \text{RMSE} \rangle$ of the closure method (with label 'cl') for the Kolmogorov flow, varying ω , and (c) the comparison between the $\langle \text{RMSE} \rangle$ of the truncation and the closure methods at $t = 100$ as a function of ω .

We conclude that the Carleman truncation(closure) at second order does not introduce any error beyond the one inherent to the lattice Boltzmann procedure, at least up to $\text{Re} \sim O(100)$. While still far from turbulence, this is nonetheless encouraging, also in view of the fact that there are interesting and demanding problems in the physics of low-Reynolds fluids, particularly in the context of biology and soft matter^{21,32}, and in quark-gluon plasma

hydrodynamics³³.

VI. QUANTUM CIRCUIT

In the previous section we have shown the performance of the CL as applied to the LBM. We have seen that, even truncating the number of Carleman variables at just second order, the error is about 10^{-3} .

However, the number of Carleman variables increases as $\mathcal{O}(N^k Q^k)$, k being the truncation order, since we need to multiply together all possible combinations of distributions functions with different velocity at different spatial lattice locations.

To convey a concrete idea of the numbers in play, we observe that a simulation of the D2Q9 model on a 32×32 square lattice implies a number of natural variables $n_v = N \times Q = 9216$, a number of Carleman variables at second order $n_{\text{CL}}^{(2)} \approx 9 \times 10^7$ and at third order $n_{\text{CL}}^{(3)} \approx 8 \times 10^{11}$. As a touchstone, the current near-exascale supercomputers can handle of the order of trillion (10^{12}) grid points. Clearly, CL is not a viable option on classical computers: the dimensionality and nonlocality price is much higher than the linearity gain.

One may argue that for each time step, the only non-local terms that affect the dynamics are the ones involving neighbor sites, which would substantially reduce the number of Carleman variables.

However, non-local correlations, involving neighbors up to order s are required, if the simulation is run as a single update from time t to time $t+s$. For instance, when a non-local variable g is calculated through the collision process, it streams into the neighboring sites serving as initial data for the subsequent collision process. Figure 5 illustrates the flow of the two points non-local function $g(x_1, y_1)$ until it converges at the point x_3 , thereby defining the local function $g(x_3, x_3)$.

The numbers provided above correspond to the global case $s \geq \frac{L+1}{2}$, where L is the linear size of the spatial domain. The situation changes if one aims to compute a number of time steps $s < \frac{L+1}{2}$. The number of variables reduces to $N(Q + Q^2(1 + 2(s-1))^2)$. For a single time step this simplifies to $n_{\text{CL}} = N(Q + Q^2)$, a significant reduction of variables.

Nevertheless, the purpose of CL is to explore whether a quantum computer could do away with the above problems, and for the application on quantum computers, it may be more convenient to deal with a high number of variables than to reset the calculation and

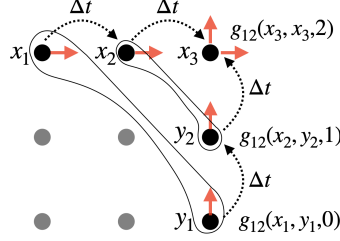


FIG. 5. The two-point non-local function $g(x_1, y_1, 0)$ at $t = 0$ streams to neighboring sites after one time step Δt , thus defining the non-local functions $g(x_2, y_2, 1)$. After one more time step, the streaming lands into the local pair function $g(x_3, x_3, 2)$ at $t = 2$.

reinitialize the quantum state³⁴. At the same time, dealing with a single time step leads to significant simplifications, to be detailed shortly.

Future quantum computers might be able to handle this explosive increase of variables in case of large time-steps simulation, as they would need a number of qubits $q = \log_2 n_{\text{CL}}$. This translates into only about $q = 27$ for the truncation at second order, and $q = 40$ for the truncation at third order, both numbers being well within the *nominal* reach of current quantum computers.

A. The quantum embedding

We can embed the whole Carleman vector with amplitude encoding in a quantum state in the following way. To embed the linear components f we can use two quantum registers, such that

$$|f\rangle = \sum_{i=0}^{Q-1} \sum_{x=0}^{N-1} f_i(x) |i\rangle_{v_1} |x\rangle_{p_1}, \quad (29)$$

where the subscripts v_1, p_1 stand for velocity and position registers respectively. The register v is composed by $\lceil \log_2 Q \rceil$ qubits, while the register p by $\lceil \log_2 N \rceil$ qubits. To embed the quadratic components g we use four quantum registers, such that

$$|g\rangle = \sum_{i,j=0}^{Q-1} \sum_{x,y=0}^{N-1} g_{ij}(x, y) |i\rangle_{v_1} |j\rangle_{v_2} |x\rangle_p |y\rangle_p, \quad (30)$$

and the same embedding strategy can be applied for functions of higher degree. In order to assemble the Carleman vector collecting together f and g , we use an extra quantum register that contains the information about the truncation order τ . This is made by $\lceil \log_2 \tau \rceil$ qubits

(just 1 qubit is necessary to embed the truncation at second order). Thus, the two vectors can be merged together

$$f \rightarrow |f\rangle|0\rangle_{v_2}|0\rangle_{p_2}|0\rangle_\tau, \quad (31)$$

$$g \rightarrow |g\rangle|1\rangle_\tau. \quad (32)$$

Although this embedding doesn't fill all the components of the quantum state, it provides a helpful way to define the streaming and collision operators. In the remaining of this section we propose a concrete way to implement the streaming and collision steps of LBM with CL in terms of quantum operators.

B. The Multi-streaming operator

In this section we analyze the streaming step of the LBM and its effect on the Carleman variables.

The linear components of the Carleman vector V, V^* of equation (16), before and after collision respectively, f, f^* , are $N \times Q$, where $N = N_x N_y$ is the number of lattice sites. For these variables, the streaming is simply given by Eq.(11). We can define S_i as the linear operator embedding the transformation to be applied to the linear components f_i^* with velocity c_i . The streaming operation can thus be written as

$$f(t + \Delta t) = \bigoplus_{i=0}^{Q-1} S_i f_i^*(t). \quad (33)$$

where \bigoplus is the symbol of the direct sum, i.e. each streaming operator S_i acts only on the subspace of the functions f_i and performs the shift $f_i(x, t + \Delta t) = f_i^*(x - c_i, t)$.

The streaming operation S_i is therefore a controlled operation, conditioned by the value of the velocity register v_1 . The explicit form of the streaming operators S_i can be obtained from an adaptation of the circuit proposed in¹⁰, that uses just a polynomial number of two-qubit gates per streaming operator.

We can consistently define the vector of the second order Carleman variables before and after collision g, g^* , where the quadratic components are given by all the possible pairs of Q and N , as stated before. The streaming on the quadratic component g_{ij} at position (x_1, x_2) applies the transformation

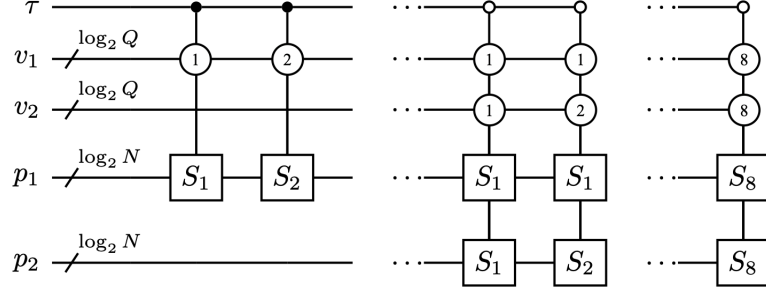


FIG. 6. The circuital representation of the streaming process for a Carleman truncation at second order. In this case the quantum register τ consists of just one qubit. When the value of the τ qubit is 0, the streaming operator is applied on the first position register controlled by a value of the first velocity register. When the value of the τ qubit is 1, two streaming operators are applied controlled by the values of two velocity registers.

$$g_{ij}(x_1, x_2, t + \Delta t) = g_{ij}^*(x_1 - c_i, x_2 - c_j, t), \quad (34)$$

and the corresponding operator is given by the tensor product of the linear streaming operators as

$$g(t + \Delta t) = \bigoplus_{i,j=0}^{Q-1} S_i \otimes S_j g_{ij}^*(t). \quad (35)$$

From the circuital point of view, the streaming operator $S_i \otimes S_j$ is a double-controlled operation conditioned by the velocity registers v_1 and v_2 . In fact, the tensor product in Eq. (35) means that we can just apply linear streaming operators on the different position registers, as depicted in Fig. 6.

As the two velocity registers run over $\log_2 Q$ qubits, we have introduced the symbol for a multi-qubit controlled operation, conditioned by the numerical value of the $Q - bit$ string. In Fig. 7 we explicitly define the symbol for a simple case of two qubits acting as control.

Furthermore, we see that the streaming in the diagonal direction, i.e. the one carried by the velocities c_5, c_6, c_7 and c_8 , cf. Table I, can be written as the composition of two streaming operators in horizontal and vertical direction, so that

$$S_5 = S_1 S_2, \quad S_6 = S_2 S_3, \quad S_7 = S_3 S_4, \quad S_8 = S_4 S_1. \quad (36)$$

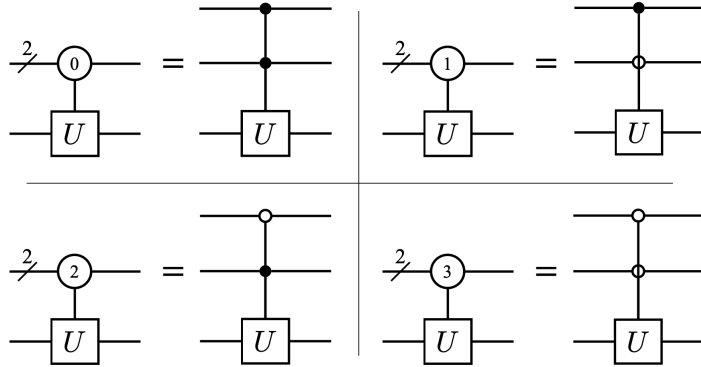


FIG. 7. The symbol for the multi-qubit controlled operation conditioned by the numerical value of the bit string for a simple scenario with two qubits as control.

The explicit form of the bi-streaming operator allows us to extend its representation to higher Carleman orders. For instance, the streaming of the cubic components of the Carleman vector is given by the tensor product of three streaming operators, as

$$h(t + \Delta t) = \bigoplus_{i,j,k=0}^{Q-1} S_i \otimes S_j \otimes S_k h_{ijk}^*(t), \quad (37)$$

and the extension applies naturally to Carleman variables of higher order.

We notice that when performing the collision step, we need to calculate also the product of functions at different lattice sites, as it is explicitly apparent from Eq. (35). The application of the bi-streaming operator requires a non-local collision operator, i.e. we need to calculate also the combinations $g^*(x_1, x_2)$ for each pair of grid points. This is of course a major downside of CL as a quantum computing method, one that complicates the circuital expression of the collision operator, as we are going to show next.

C. The collision operator

The collision step of the LBM is a non-linear operation that implements the relaxation of the probability distributions towards the equilibrium distributions (12). By definition, the dissipative process induced by the relaxation cannot be represented by a circuit performing unitary operations. However, we can circumvent this issue by using an ancilla qubit and making use of open quantum system theory. We can therefore implement a circuit that allows only unitary operations, but where only a subset of the available qubits is accounted

for (the system). By tracing out the ancilla qubits (environment), we obtain a non-unitary operation on the system qubits.

The circuit that implements the collision operator is detailed in Ref.²⁶. This circuit is capable of performing non-unitary operations on the qubits by means of an ancilla qubit. It achieves this by decomposing a non-unitary, positive-definite matrix C into a linear combination of two unitaries U_a and U_b , such that

$$C = U_a + \gamma U_b. \quad (38)$$

The coefficient γ is chosen such that the maximum eigenvalue of C , c_M , fulfills the relation $c_M \leq 1 + \gamma$. Moreover, a requirement needed to apply this decomposition is that $c_M - c_m < 2$, where c_m is the minimum eigenvalue of C . Whenever this is not the case, we can define a renormalized matrix $\tilde{C} = C/c_M$ and apply the decomposition to the new matrix. The coefficient has to be set to $\gamma = 1 - c_m/c_M$ ²⁶.

The circuit is represented in Fig. 8. The Carleman vector is embedded in the state $|\psi\rangle$, and an ancilla qubit is initialized in $|0\rangle_a$. We perform an R_y rotation of angle $\Gamma = \arccos\left(\sqrt{\frac{\gamma}{\gamma+1}}\right)$, on the ancilla qubit, yielding the state $|\psi\rangle(\cos\Gamma|0\rangle_a + \sin\Gamma|1\rangle_a)$. The action of the anti-controlled and controlled unitaries leads to the state $U_b|\psi\rangle\cos\Gamma|0\rangle_a + U_a|\psi\rangle\sin\Gamma|1\rangle_a$ and the inverse rotation $R_y^\dagger(\Gamma)$ on the ancilla qubit results into

$$\frac{1}{\gamma+1}|0\rangle(U_a + \gamma U_b)|\psi\rangle + \frac{\sqrt{\gamma}}{\gamma+1}|1\rangle(U_a - U_b)|\psi\rangle. \quad (39)$$

We finally measure the ancilla qubit. If the outcome is $|0\rangle$, the state collapses onto $(U_a + \gamma U_b)|\psi\rangle$, which is exactly the application of C on the state ψ . In this case, the algorithm succeeds and we can proceed with the streaming step. On the other hand, if the outcome of the measurement is 1, the update fails and the circuit needs to be repeated. The probability of success is constrained by $p_0 \leq \frac{4\gamma}{(\gamma+1)^2}$.

Inspection of the collision matrix shows that it can be explicitly written as follows:

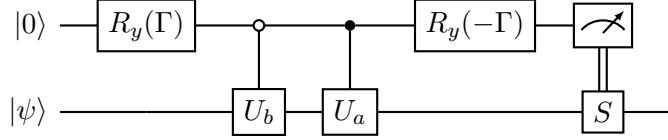


FIG. 8. The circuit for the implementation of the collision step. The initial state $|\psi\rangle$ contains the collection of the Carleman variables. Depending on the result of the measurement on the ancilla qubit, the algorithm is successful and the streaming operator S is applied.

$$\begin{aligned}
\mathcal{C} = & |0\rangle\langle 0|_{\tau} \otimes \mathbb{1}_{p_1} \otimes \sum_{ij} A_{ij} |i\rangle\langle j|_{v_1} \otimes |0\rangle\langle 0|_{p_2} \otimes |0\rangle\langle 0|_{v_2} + \\
& |0\rangle\langle 1|_{\tau} \otimes \mathbb{1}_{p_1} \otimes \sum_{ijk} B_{ijk} |i\rangle\langle j|_{v_1} \otimes \sum_x |0\rangle\langle x|_{p_2} \otimes |0\rangle\langle k|_{v_2} + \\
& |1\rangle\langle 1|_{\tau} \otimes \mathbb{1}_{p_1} \otimes \sum_{ik} A_{ik} |i\rangle\langle k|_{v_1} \otimes \mathbb{1}_{p_2} \otimes \sum_{jl} A_{jl} |j\rangle\langle l|_{v_2},
\end{aligned} \tag{40}$$

or, in more compact form:

$$\mathcal{C} = \begin{pmatrix} \mathcal{A} \otimes |0\rangle\langle 0|_{p_2} \otimes |0\rangle\langle 0|_{v_2} & \mathcal{B} \otimes \sum_x |0\rangle\langle x|_{p_2} \\ 0 & \mathcal{A} \otimes \mathcal{A} \otimes \mathbb{1}_{p_2} \end{pmatrix} \otimes \mathbb{1}_{p_1}, \tag{41}$$

where \mathcal{A} and \mathcal{B} represent the A and B matrices of Eq. (15) embedded in the space of qubits. The different quadrants of the matrix (41) refer to the values of the τ register. We note that all the components depend in a non-trivial way on the p_2 register. This does not permit to define the collision operator as a local process to be applied only on the velocity registers v_1 and v_2 , a feature which is rooted in the inherent non-locality of the Carleman linearization. Because of this, the matrix cannot be written in sparse, block-diagonal form, a well known requirement for polynomial approximations in the number of quantum gates^{35,36}. Thus, the two controlled operations of the unitaries U_a, U_b require a number of two-qubit gates of the order of 4^n , according to the theoretical lower bound³⁷. Since the number of qubits in our system is $n = \lceil \log_2(NQ + N^2Q^2) \rceil + 1$, for a Carleman system truncated at second order, the corresponding number of two-qubit gates scales as $\mathcal{O}(N^4Q^4)$.

For relevant cases, this number exceeds by several orders of magnitude the current capacity of any quantum computer^{22,38}. Just a simple 32×32 grid with 9 discrete populations, features $(NQ)^4 \sim 9000^4 \sim 10^{16}$ two-qubit gates.

We numerically tested this result for the circuit of the collision operator with the IBM

Qiskit package. To streamline the numerical analysis, we define an hermitian augmented Carleman matrix \mathcal{C}^H as;

$$\mathcal{C}^H = \begin{pmatrix} 0 & \mathcal{C} \\ \mathcal{C}^T & 0 \end{pmatrix}. \quad (42)$$

where superscript T stands for “transpose”.

This passage simplifies the numerical representation of \mathcal{C}^H as the weighted sum of unitary matrices (Eq. (38)) with the minimal addition of just one qubit. With this matrix at hand, we can translate the circuit into a sequence of two-qubit gates using Qiskit’s decomposition tool. This straightforward step gives a number of two-qubit gates close to the theoretical lower-bound mentioned earlier, indicating that simplifying the circuit is by no means a trivial task. We stress here that this issue is common to any algorithm which aims at implementing a non-sparse matrix.

1. Single time-step collision operator

A possible getaway from this issue is to introduce a *single-step* collision operator. As highlighted in section VI, the non-local Carleman variables are needed only if one aims to apply the dynamics over multiple time steps. However, if only one single time step is implemented, the number of Carleman variables reduces to $N(Q + Q^2)$. Since all the Carleman variables are now local, the quantum register p_2 can be dropped, and the matrix (41) takes the simpler form:

$$\mathcal{C}_{s=1} = \begin{pmatrix} \mathcal{A} \otimes |0\rangle\langle 0|_{v_2} & \mathcal{B} \\ 0 & \mathcal{A} \otimes \mathcal{A} \end{pmatrix} \otimes \mathbb{1}_{p_1}, \quad (43)$$

which is also local in qubit’s space. This means that we can apply the collision operator only on the registers embedding the information about truncation order τ and the velocities v_1, v_2 .

In this framework, we can exploit the symmetry of the second order functions, such that $g_{ij} = g_{ji}$, to reduce even further the dimension of the number of Carleman variables to $\frac{3}{2}NQ + \frac{NQ^2}{2}$. Consequently, for the D2Q9 model, the matrix $\mathcal{C}_{s=1}$ of Eq. (43) can be written with 54 variables, and be embedded in the space of $q = 6$ qubits, *regardless of the number*

of lattice sites.

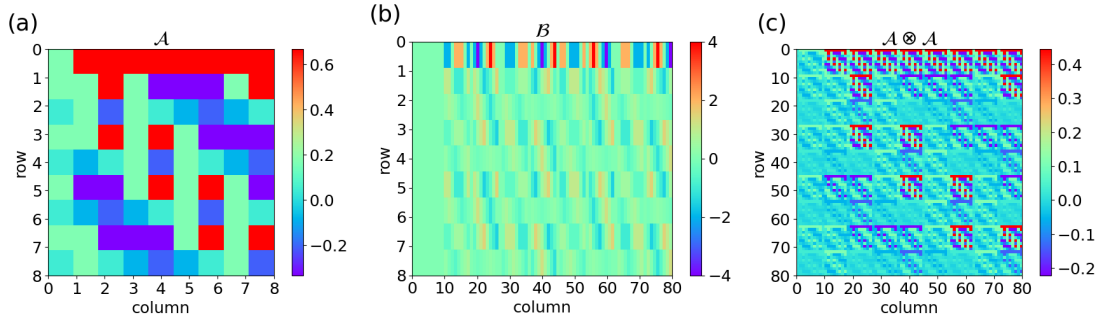


FIG. 9. The shape and the order of magnitude of the matrices \mathcal{A}, \mathcal{B} and $\mathcal{A} \otimes \mathcal{A}$ in (a), (b) and (c) respectively. Together they form the matrices (41) and (43).

Figures 9(a) and (b) show the matrices of Eqs. (41) and (43) in the case of a single lattice site respectively. We remind that for any lattice with some spatial extension, the matrix \mathcal{C} is not further reducible, implying that the number of two-qubit gates grows exponentially with n , whereas for the single time-step case, the matrix $\mathcal{C}_{s=1}$ is encoded within a fixed number of gates, for any number of lattice sites, thus making it exponentially more efficient than any classical algorithm.

We tested with Qiskit the number of two-qubit gates needed to construct the single step circuit. A number of two-qubit gates of the order of $4^7 = 16384$ is needed to produce both the controlled U_a and U_b of the circuit, yielding a total value about $\sim 30,000$ two-qubit gates. Although this number is too large for present-day quantum hardware, it might become viable in the near or mid-term.

As is well known, the downside of any single time-step implementation, not just the Carleman LB algorithm discussed here, is the overhead due to the embedding and readout processes, that need to be repeated at every single timestep, thereby spoiling the quantum advantage. These are important issues that need to be addressed in future work.

Looking at Fig. 9(a), we see the specific symmetries of the non-local operator C could lead to a lower number of gates, and therefore future work should explore the best compiling method, using several potential techniques^{39–41}, for example tensor network analysis^{42,43} to minimize non-local correlations¹⁵. Another potential route is to apply the CL procedure to the fluid equations in their native Navier-Stokes form: the Carleman matrix is seemingly more complex due to the cross-correlations between fluid density, flow and pressure, but

likely to entail a lesser number of Carleman variables, with a consequent benefit on the depth of the algorithm. Finally, also the long-known option of special-purpose quantum hardware might be worth being revisited^{18,44}.

VII. CONCLUSIONS AND OUTLOOK

In this work we have developed a Carleman linearization of the Lattice Boltzmann dynamics for a weakly-compressible fluid for both classical and quantum computers. The most promising result is that the relative error between CL–LBM is well within the “physiological” level of the standard lattice Boltzmann, method at least for moderate Reynolds numbers up to $\mathcal{O}(10 - 100)$. Although this value does not describe turbulence, it definitely displays sizeable non-linear effects, leaving hope that turbulent regimes can be attended in the future, an hypothesis that can only be tested on quantum computers.

The CL procedure becomes rapidly unfeasible on classical computers, showing that in a classical framework, trading nonlinearity for extra-dimensions is a very inconvenient bargain. In fact, the exponential increase of Carleman variables with the truncation order makes this method substantially useless for relevant applications, as the number of variables quickly reaches the limit of exascale supercomputers even on very small grids.

Nonetheless, we stress that the ultimate goal of CL is to implement the embedding of fluid dynamics onto quantum computers, where the number of qubits scales like the logarithm of the number of variables, thus taming the exponential increase of the number of Carleman variables via a suitable embedding onto qubits. To this purpose, we have proposed and described the explicit form of the quantum circuit implementing the CL procedure as applied to the Lattice Boltzmann formulation of fluids. To the best of our knowledge, this is the first work delivering an explicit formulation and implementation of the quantum algorithm into an actual quantum circuit. Specifically, we have derived the circuit for both the streaming and the collision operators and combined them in terms of global unitary gates. The latter circuit faces with a formidable depth problem, scaling like $(NQ)^4$, seemingly unviable on any quantum computer, unless dramatic improvements on error correction/mitigation procedures are achieved in the coming years. However, this steep barrier can be tamed by turning to single-step formulations, featuring a fixed circuit depth, regardless of the number of lattice sites. Developing an efficient multi-step formulation stands out as a major

challenge for the Carleman approach to quantum computing of fluids.

Among prospective directions to be explored, we mention the Carleman procedure applied to the native Navier-Stokes formulations, concrete applications of the Solovay-Kitaev theorem, tensor-network analysis or the use of parametric quantum circuits. Finally, special-purpose quantum computers for fluid might also be worth revisiting.

ACKNOWLEDGMENTS

We acknowledge financial support from National Centre for HPC, Big Data and Quantum Computing (Spoke 10, CN00000013). We also acknowledge the CERN and IBM Quantum Hub with which the Italian Institute of Technology (IIT) is affiliated. The authors gratefully acknowledge discussions with M. Maronese, A. Solfanelli, R. Steijl, K. Sreenivasan and W. Itani.

The authors have no conflicts to disclose. The data that support the findings of this study are available from the corresponding author upon reasonable request.

REFERENCES

- ¹M.A. Nielsen and I.L. Chuang. *Quantum Computation and Quantum Information: 10th Anniversary Edition*. Cambridge University Press, 2010.
- ²Aram W. Harrow, Avinatan Hassidim, and Seth Lloyd. Quantum Algorithm for Linear Systems of Equations. *Physical Review Letters*, 103(15):150502, October 2009.
- ³Tameem Albash and Daniel A. Lidar. Adiabatic quantum computation. *Rev. Mod. Phys.*, 90:015002, Jan 2018.
- ⁴Dimitrios Giannakis, Abbas Ourmazd, Philipp Pfeffer, Jörg Schumacher, and Joanna Slawinska. Embedding classical dynamics in a quantum computer. *Physical Review A*, 105(5):052404, May 2022.
- ⁵Stefano Mangini, Alessia Marruzzo, Marco Piantanida, Dario Gerace, Daniele Bajoni, and Chiara Macchiavello. Quantum neural network autoencoder and classifier applied to an industrial case study. *Quantum Machine Intelligence*, 4(2):13, June 2022. Number: 2.
- ⁶I. M. Georgescu, S. Ashhab, and Franco Nori. Quantum simulation. *Reviews of Modern Physics*, 86(1):153–185, March 2014. Publisher: American Physical Society.

⁷Francesco Tacchino, Alessandro Chiesa, Stefano Carretta, and Dario Gerace. Quantum Computers as Universal Quantum Simulators: State-of-the-Art and Perspectives. *Advanced Quantum Technologies*, 3(3):1900052, 2020. Number: 3 eprint: <https://onlinelibrary.wiley.com/doi/pdf/10.1002/qute.201900052>.

⁸Richard P. Feynman. Simulating physics with computers. *International Journal of Theoretical Physics*, 21(6):467–488, June 1982.

⁹René Steijl. *Quantum Algorithms for Fluid Simulations*. IntechOpen, June 2019. Publication Title: Advances in Quantum Communication and Information.

¹⁰Blaga N. Todorova and René Steijl. Quantum algorithm for the collisionless Boltzmann equation. *Journal of Computational Physics*, 409:109347, May 2020.

¹¹Frank Gaitan. Finding flows of a Navier–Stokes fluid through quantum computing. *npj Quantum Information*, 6(1):1–6, July 2020. Number: 1 Publisher: Nature Publishing Group.

¹²Rene Steijl. Quantum Algorithms for Nonlinear Equations in Fluid Mechanics. In Yongli Zhao, editor, *Quantum Computing and Communications*. IntechOpen, February 2022.

¹³Xiangyu Li, Xiaolong Yin, Nathan Wiebe, Jaehun Chun, Gregory K. Schenter, Margaret S. Cheung, and Johannes Mülmenstädt. Potential quantum advantage for simulation of fluid dynamics, April 2023. arXiv:2303.16550 [physics, physics:quant-ph].

¹⁴John F. Wendt, John D. Anderson, and Von Karman Institute for Fluid Dynamics, editors. *Computational fluid dynamics: an introduction*. Springer, Berlin ; [London], 3rd ed edition, 2008. OCLC: ocn288984495.

¹⁵Sauro Succi, W. Itani, K. Sreenivasan, and R. Steijl. Quantum computing for fluids: Where do we stand? *Europhysics Letters*, 144(1):10001, October 2023. Publisher: EDP Sciences, IOP Publishing and Società Italiana di Fisica.

¹⁶Sauro Succi, Roberto Benzi, and Francisco Higuera. The lattice Boltzmann equation: A new tool for computational fluid-dynamics. *Physica D: Nonlinear Phenomena*, 47(1):219–230, January 1991.

¹⁷R. Benzi, S. Succi, and M. Vergassola. The lattice Boltzmann equation: theory and applications. *Physics Reports*, 222(3):145–197, December 1992.

¹⁸S. Succi and R. Benzi. Lattice Boltzmann equation for quantum mechanics. *Physica D: Nonlinear Phenomena*, 69(3):327–332, December 1993.

¹⁹Timm Krüger, Halim Kusumaatmaja, Alexandr Kuzmin, Orest Shardt, Goncalo Silva,

and Erlend Magnus Viggen. *The Lattice Boltzmann Method: Principles and Practice*. Graduate Texts in Physics. Springer International Publishing, Cham, 2017.

²⁰Giacomo Falcucci, Giorgio Amati, Pierluigi Fanelli, Vesselin K. Krastev, Giovanni Polverino, Maurizio Porfiri, and Sauro Succi. Extreme flow simulations reveal skeletal adaptations of deep-sea sponges. *Nature*, 595(7868):537–541, July 2021. Number: 7868 Publisher: Nature Publishing Group.

²¹Sauro Succi. *The Lattice Boltzmann Equation: For Complex States of Flowing Matter*. Oxford University Press, Oxford, New York, April 2018.

²²Sergey Bravyi, Oliver Dial, Jay M. Gambetta, Darío Gil, and Zaira Nazario. The future of quantum computing with superconducting qubits. *Journal of Applied Physics*, 132(16):160902, October 2022.

²³Torsten Carleman. Application de la théorie des équations intégrales linéaires aux systèmes d'équations différentielles non linéaires. *Acta Mathematica*, 59(none):63–87, January 1932. Publisher: Institut Mittag-Leffler.

²⁴K Kowalski and W-H Steeb. *Nonlinear Dynamical Systems and Carleman Linearization*. WORLD SCIENTIFIC, March 1991.

²⁵Wael Itani and Sauro Succi. Analysis of Carleman Linearization of Lattice Boltzmann. *Fluids*, 7(1):24, January 2022. Number: 1 Publisher: Multidisciplinary Digital Publishing Institute.

²⁶A. Mezzacapo, M. Sanz, L. Lamata, I. L. Egusquiza, S. Succi, and E. Solano. Quantum Simulator for Transport Phenomena in Fluid Flows. *Scientific Reports*, 5(1):13153, August 2015. Number: 1 Publisher: Nature Publishing Group.

²⁷Jin-Peng Liu, Herman Øie Kolden, Hari K. Krovi, Nuno F. Loureiro, Konstantina Trivisa, and Andrew M. Childs. Efficient quantum algorithm for dissipative nonlinear differential equations. *Proceedings of the National Academy of Sciences*, 118(35):e2026805118, August 2021. Publisher: Proceedings of the National Academy of Sciences.

²⁸Wael Itani, Katepalli R. Sreenivasan, and Sauro Succi. Quantum Algorithm for Lattice Boltzmann (QALB) Simulation of Incompressible Fluids with a Nonlinear Collision Term, April 2023. arXiv:2304.05915.

²⁹Si Bui Quang Tran, Fong Yew Leong, Quang Tuyen Le, and Duc Vinh Le. Lattice Boltzmann Method for high Reynolds number compressible flow. *Computers & Fluids*, 249:105701, December 2022.

³⁰S. Succi. *The Lattice Boltzmann Equation: For Fluid Dynamics and Beyond*. Clarendon Press, June 2001. Google-Books-ID: OC0Sj_xgnhAC.

³¹Cyrus K. Aidun and Jonathan R. Clausen. Lattice-Boltzmann Method for Complex Flows. *Annual Review of Fluid Mechanics*, 42(1):439–472, 2010. eprint: <https://doi.org/10.1146/annurev-fluid-121108-145519>.

³²Burkhard Dünweg and Anthony J. C. Ladd. Lattice Boltzmann Simulations of Soft Matter Systems. In Christian Holm and Kurt Kremer, editors, *Advanced Computer Simulation Approaches for Soft Matter Sciences III*, Advances in Polymer Science, pages 89–166. Springer, Berlin, Heidelberg, 2009.

³³M. Mendoza, B. M. Boghosian, H. J. Herrmann, and S. Succi. Fast Lattice Boltzmann Solver for Relativistic Hydrodynamics. *Physical Review Letters*, 105(1):014502, June 2010. Publisher: American Physical Society.

³⁴Christa Zoufal, Aurélien Lucchi, and Stefan Woerner. Quantum Generative Adversarial Networks for learning and loading random distributions. *npj Quantum Information*, 5(1):1–9, November 2019. Number: 1 Publisher: Nature Publishing Group.

³⁵Dominic W. Berry, Graeme Ahokas, Richard Cleve, and Barry C. Sanders. Efficient Quantum Algorithms for Simulating Sparse Hamiltonians. *Communications in Mathematical Physics*, 270(2):359–371, March 2007.

³⁶Stephen P. Jordan and Paweł Wocjan. Efficient quantum circuits for arbitrary sparse unitaries. *Physical Review A*, 80(6):062301, December 2009.

³⁷Adriano Barenco, Charles H. Bennett, Richard Cleve, David P. DiVincenzo, Norman Margolus, Peter Shor, Tycho Sleator, John A. Smolin, and Harald Weinfurter. Elementary gates for quantum computation. *Physical Review A*, 52(5):3457–3467, November 1995.

³⁸Swami T. Tannu and Moinuddin K. Qureshi. Not All Qubits Are Created Equal: A Case for Variability-Aware Policies for NISQ-Era Quantum Computers. In *Proceedings of the Twenty-Fourth International Conference on Architectural Support for Programming Languages and Operating Systems*, ASPLOS ’19, pages 987–999, New York, NY, USA, April 2019. Association for Computing Machinery.

³⁹V.V. Shende, S.S. Bullock, and I.L. Markov. Synthesis of quantum-logic circuits. *IEEE Transactions on Computer-Aided Design of Integrated Circuits and Systems*, 25(6):1000–1010, 2006.

⁴⁰Péter Rakyta and Zoltán Zimborás. Approaching the theoretical limit in quantum gate

decomposition. *Quantum*, 6:710, May 2022. Publisher: Verein zur Förderung des Open Access Publizierens in den Quantenwissenschaften.

⁴¹Liam Madden and Andrea Simonetto. Best Approximate Quantum Compiling Problems. *ACM Transactions on Quantum Computing*, 3(2):7:1–7:29, March 2022.

⁴²Timo Felser, Simone Notarnicola, and Simone Montangero. Efficient Tensor Network Ansatz for High-Dimensional Quantum Many-Body Problems. *Physical Review Letters*, 126(17):170603, April 2021. Publisher: American Physical Society.

⁴³Niall F. Robertson, Albert Akhriev, Jiri Vala, and Sergiy Zhuk. Approximate Quantum Compiling for Quantum Simulation: A Tensor Network based approach, March 2023. arXiv:2301.08609 [quant-ph].

⁴⁴Jeffrey Yepez. Quantum Lattice-Gas Model for the Burgers Equation. *Journal of Statistical Physics*, 107(1):203–224, April 2002.